An Empirical Model for Television Frequency Interference Correction of AMSR2 Data Over Ocean Near the U.S. and Europe

Xiaoxu Tian and Xiaolei Zou

***Abstract*—Television (TV) radio frequency interference (TFI) signals are found in the Advanced Microwave Scanning Radiometer 2 (AMSR2) observations of those channels with their frequencies centered at 18.7- or 10.65-GHz frequencies over coastal regions near the U.S. and Europe, respectively. When TV signals are reflected off the ocean surface and get into AMSR2 field of views, the AMSR2-measured radiance contains not only information of natural emission from Earth's surface but also the reflected TV signals. If not detected and corrected, TFI introduces errors into the geophysical retrieval products. The occurrence and intensity of TFI are determined by the angle between the observation beam vector and the reflected TV signal vector (i.e., TFI glint angle) and the background TV signal intensity. In this paper, an empirical model is developed to quantitatively calculate the contribution of TFI signals to AMSR2 observations based on TFI glint angle and TV signal intensity. This empirical model is then applied to AMSR2 K-band channels over North America and X-band channels over Europe. It is shown that the annual mean bias for the TFI-affected observations of the 18.7-GHz channel at horizontal (vertical) polarization reduces from a value of more than 5 K (2 K) to about −0.5 K (0.5) after TFI correction over the coastal ocean near North America. The annual mean bias for the TFI-affected observations of the 10.65-GHz channel at horizontal (vertical) polarization reduces from a value of about 2.5 K to about −0.7 K (0.5 K) after TFI correction over the coastal ocean near Europe. False maxima in AMSR2-retrieved cloud liquid water path and dry anomalies in AMSR2-retrieved total precipitable water near the coastal regions are also eliminated after incorporating the TFI correction.**

***Index Terms*—Advanced Microwave Scanning Radiometer 2 (AMSR2), K-band, television frequency interference (TFI), X-band.**

I. Introduction

THE Advanced Microwave Scanning Radiometer 2 (AMSR2) is onboard the Global Change Observation Mission—Water 1 (GCOM-W1) satellite, which was successfully launched onto a sun-synchronous orbit at an altitude of 705 km on May 17, 2012. As the successor of AMSR-E carried by Aqua satellite, AMSR2 inherited all AMSR-E's channels from 6.925 to 89.0 GHz, and it has an additional pair of dual-polarized channels with center frequencies at 7.3 GHz [1]. The purpose of adding the 7.3-GHz channels is for mitigating radio frequency interference (RFI). Other passive microwave conical-scanning radiometer instruments similar to AMSR-E include the WindSat radiometer onboard the Coriolis satellite and the Microwave Radiation Imager onboard the FY3B and FY3C satellites. The 6.926 (C-band), 10.65 (X-band), and 18.7 (K-band) channels of these instruments can be applied for retrievals of geophysical variables over both ocean [2] and land [3]–[5]. However, these low-frequency channels are located in unprotected bands and are exposed to signals from ground-based and/or space-based military or commercial active sensors [6]–[8].

Over ocean, the primary source of interference is the geostationary TV satellites that transmit TV signals at frequencies that are within the bandwidth of radiometer channels [9], [10]. The ocean surface has a relatively higher reflectivity compared with that of the land surface due to a high permittivity of seawater. When the TV signals transmitted by the geostationary satellite reach the sea surface, a portion of the signals could be reflected back toward space. When a radiometer's antenna happens to be facing the reflected signal, these reflected TV signals will be mixed with the natural radiation emitted by the Earth surface (Fig. 1). The interferences of the radiance measurements from the meteorological satellite radiometric instruments with TV signals reflected off the ocean surface are known as television frequency interferences (TFIs). In Europe, over five TV satellites are operating at X-bands that overlap with the AMSR2 10.65-GHz channels. Over North America, the DirecTV satellite groups operate at frequencies close to the K-band channels of radiometers [11], [12]. The occurrence of TFI, if not detected and corrected, would introduce erroneous information into radiance observations and then to AMSR2-retrieved geophysical products, such as total precipitable water (TPW), liquid water path (LWP), sea surface wind (SSW), and sea surface temperatures (SSTs) [12]–[14].

Numerous previous studies had attempted to identify the TFI among observations in order to minimize the detrimental impacts of TFI on meteorological satellite observations. Li *et al.* [15] proposed a regression method to predict the TFI-free brightness temperature for the interfered channels with the aid of other channels. The accuracies of such regression-predicted brightness temperature are promising. However, derivations of the regression coefficients require observation data from a long time period (e.g., six months in [15]).

Manuscript received July 3, 2015; revised November 23, 2015; accepted February 8, 2016. Date of publication March 28, 2016; date of current version May 24, 2016. This work was supported by NOAA Proving Ground and Risk Reduction (PGRR) Program Project (NA11OAR4320199) and Hurricane Forecast Improvement Program (HFIP) Project (NA15NWS4680002).

The authors are with the Earth System Science Interdisciplinary Center, University of Maryland, College Park, MD 20740-3823 USA (e-mail: xzou1@umd.edu).

Digital Object Identifier 10.1109/TGRS.2016.2529504

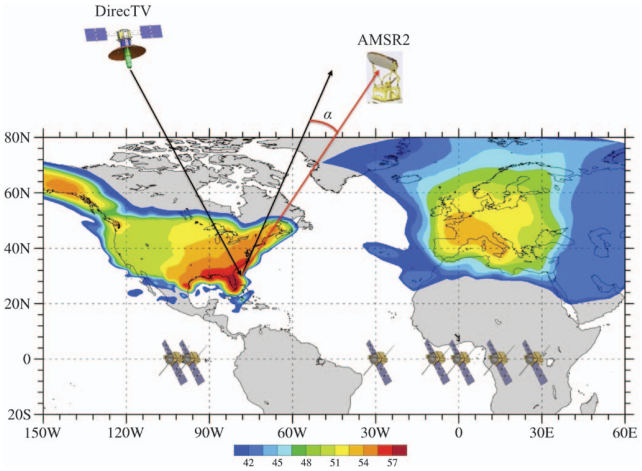

Fig. 1. Radio signal intensity (unit: dBW) from DirecTV-11 located at 102.8° W and Eutelsat 13B at 13.5° E (color shading) (http://www.satbeams.com/footprints?beam=6219), as well as a schematic illustration of the reflection of TV signals (black arrow) off the ocean surface, an Earth emission into the AMSR2 field of view (red arrow), and the glint angle (α). The locations of two geostationary satellites over the U.S. (DirecTV-11 and DirecTV-12) and five geostationary satellites over Europe (Hispasat 1E, Eutelsat West 7A, Thor 6, Hot Bird 13B, and Astra 2E) located above the equator are indicated by a schematic satellite image.

Adams *et al.* [9] developed an algorithm to detect the interference based on the goodness-of-fit between the modeled and measured brightness temperatures, which is essentially chi-square probability. Reference [19] pointed out an existence of TFI signals at K band over land that could be reflected by snow surfaces based on the maximum differences of brightness temperature measurements between 19 and 22 GHz at the same polarization over a winter month period. In this paper, an empirical model is developed for evaluating the occurrence and intensity of TFI over ocean. This model is based on the same principle that was used by Yang and Weng [16] for mitigation of lunar contamination in the Advanced Technology Microwave Sensor (ATMS) observations. A quantitative determination of TFI contribution to an AMSR2 observation can be derived given the TFI glint angle, which is defined as the angle between the direction that the radiometer's antenna faces and the direction of the reflected TV signal, latitude, longitude, sensor zenith, and sensor azimuth angles of the AMSR2 observation as well as the background TV signal intensity of each relevant geostationary TV satellite that could be affecting the area of interest. The calculation of TFI correction using this empirical model does not involve any AMSR2 radiance observations, as did the earlier methods.

This paper is organized as follows. The AMSR2 data characteristics are described in Section II. A detailed description of the TFI correction model is given in Section III. The numerical results from the TFI correction model are discussed in Section IV. Section V provides the summary and concludes.

II. AMSR2 Channel Characteristics and Geophysical Retrieval Products

AMSR2 is the only instrument onboard the Global Change Observing Mission—Water satellite, which was successfully launched on May 17, 2012, onto a sun-synchronous orbit at 705-km altitude. It is the successor of the Advanced Microwave Scanning Radiometer—EOS (AMSR-E), which ceased to operate on October 4, 2011. AMSR2 retains the same conical scan feature as AMSR-E with a constant local zenith angle of 55°. Its swath width is 1450 km. AMSR2 has a total of 14 dual-polarized channels with 7 center frequencies located at 6.925, 7.3, 10.65, 18.7, 23.8, 36.5, and 89.0 GHz. Compared with AMSR-E, the two 7.3-GHz channels are newly added for a more effective detection and mitigation of RFI signals over land. The bandwidth, beamwidth, along-track and across-track sizes of an instantaneous field of view (IFOV), noise equivalent differential temperature (NEDT), and sampling interval are provided in Table I.

TABLE I
AMSR2 Instrument Characteristics

Channel Frequency [GHz]	Band Width [MHz]	Beam Width [deg]	IFOV [km]	NEDT [K]	Sampling Interval [km]	Pol.
6.925	350	1.8	35×62	0.34	10	H/V
7.3	350	1.8	34×58	0.43		
10.65	100	1.2	24×42	0.7		
18.7	200	0.65	14×22	0.7		
23.8	400	0.75	15×26	0.6		
36.5	1000	0.35	7×12	0.7		
89.0	3000	0.15	3×5	1.2	5	

Over ocean, the TFI-contaminated channels include those at 10.65 GHz over Europe and 18.7 GHz over North America. Along with the 36.5-GHz channels, the AMSR2 radiance observations at the 10.65-GHz channels are used for retrieving SSWs [14]. Combined with the 6.925-GHz channels, the AMSR2 radiance observations at the 10.65-GHz channels are also used for generating SST products [14]. The AMSR2 channels at 18.7 GHz are used for retrieval of both cloud LWP and TPW [13].

III. Empirical Model for TFI Correction

A. Empirical Model for TFI Correction Over the U.S.

TFI is caused by the ocean-reflected TV energy entering AMSR2's antenna. Physically, it is similar to a lunar contamination in ATMS observations caused by the lunar radiation entering into the ATMS antenna. Yang and Weng [16] found that the brightness temperature increment from the lunar contamination could be expressed as a function of the antenna response function, solid angle of the moon, and microwave radiance of the moon disk. The solid angle and microwave radiance of the moon disk together determine the amplitude. The antenna response within the mean beam range can be accurately simulated by a 1-D Gaussian function [18]. An empirical model similar to a lunar correction model is developed for TFI correction. It is based on the fact that the antenna response to either of the reflected TV energy is, in principle, the same process as lunar contamination. Over the U.S., there are two geostationary TV satellites: DirecTV-11 and DirecTV-12. DirecTV-12 is located at 102.8° W, and

DirecTV-11 is located at 99.2° W. The change of the brightness temperature at 18.7 GHz ($\Delta T_{b,18p}^{\mathrm{TFI}}$) is

$$\Delta T_{b,18p}^{\mathrm{TFI,phy}} = \Omega_{\mathrm{TV11},p} \exp\left(\frac{-\alpha_{\mathrm{TV11}}^2}{2\sigma_{\mathrm{TV11}}^2}\right) + \Omega_{\mathrm{TV12},p} \exp\left(\frac{-\alpha_{\mathrm{TV12}}^2}{2\sigma_{\mathrm{TV12}}^2}\right) \quad (1)$$

where p denotes either vertical or horizontal polarization; $\Omega_{\mathrm{TV11},p}$ and $\Omega_{\mathrm{TV12},p}$ are the background TFI intensities related to the TV signal strengths of DirecTV-11 and DirecTV-12 and have the same physical unit as the brightness temperatures, respectively; σ_{TV11} and σ_{TV12} are the 3-dB beamwidths of the AMSR2 antenna to the TV signals from DirecTV-11 and DirecTV-12, respectively, and quantify the sensitivity of AMSR2 to the signals from a specific TV satellite; and α_{TV11} and α_{TV12} are the AMSR2 glint angles with respect to DirecTV-11 and DirecTV-12, respectively, and represent the angle between the reflect TV signal vectors and the AMSR2 Earth scene vector. The unknown parameters $\Omega_{\mathrm{TV11},p}$, $\Omega_{\mathrm{TV12},p}$, α_{TV11}, and α_{TV12} in (1) are to be determined using AMSR2 data in 2014.

Since at a fixed location, $\Omega_{\mathrm{TV11},p}$ and $\Omega_{\mathrm{TV12},p}$ are invariant with time. Therefore, the antenna pattern parameters (σ_{TV11} and $\sigma_{\mathrm{TV12},p}$) can be first determined at two fixed locations. TFI occurs at small glint angles. In order to better fit the values of the antenna pattern parameters σ_{TV11} and σ_{TV12}, it is desirable to have enough data at small glint angles. In one hand, the geostationary satellites are fixed in space with respect to the Earth. The spatial distribution of the incident angle of a TV satellite does not vary with time. On the other hand, being a conical scanner, AMSR2 has a fixed incident angle 55° at the Earth surface. A necessary but not sufficient condition for AMSR2 glint angle to be small is that the AMSR2 pixels are located at a place where the incident angle of the geostationary satellite is close to 55°. Fig. 2(a) shows the incident angle field of DirecTV-11 (θ_{TV11}, black curve) and that of DirecTV-12 (θ_{TV12}, purple curve). The data within grid boxes A and B that are close to the 55° incident angle contour lines in a one-year period of 2014 were selected for determining the 3-dB beamwidth of the AMSR2 antenna to the TV signals from DirecTV-11 and DirecTV-12. The TV signal intensities (dBW) of DirecTV-11 and DirecTV-12 over water areas over and around the U.S. are provided in Fig. 2(b) and (c). These data are obtained from a publicly available website.[1]

Due to a close distance between DirecTV-11 and DirecTV-12, the differences of the AMSR2 glint angles with respect to two TV satellites are less than 5°. In order to isolate the effect from one satellite to the other satellite as much as possible, a further selection is made to the data in grid boxes A and B to satisfy the following requirements: 1) the differences of the glint angles between DirecTV-11 and DirecTV-12 (i.e., $\alpha_{\mathrm{TV11}} - \alpha_{\mathrm{TV12}} \leq -3.5$) are less than 3.5°; 2) the SSW speed is less than 6 m s^{-1}; 3) the LWP is less than 0.5 kg m^{-2}; and 4) the glint angles are smaller than 25°. Once the two data sets are selected, one for DirecTV-11 and the other for DirecTV-12,

[1]http://www.satbeams.com/footprints?beam=6219.

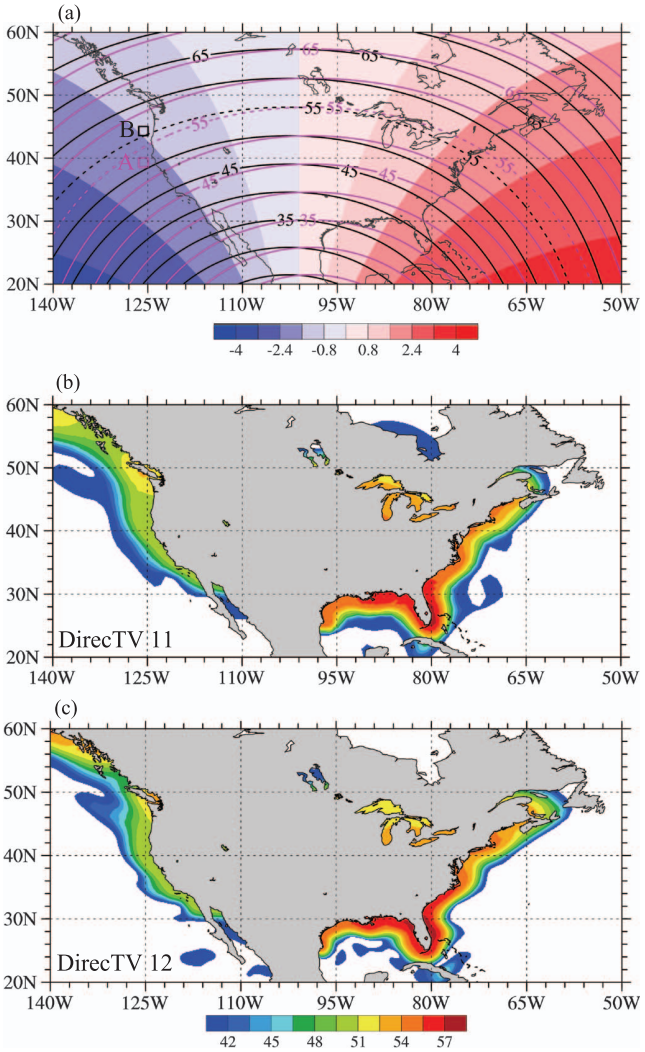

Fig. 2. (a) Spatial distributions of the incident angles (unit: degrees) of DirecTV-11 (θ_{TV11}, black curve) and DirecTV-12 (θ_{TV12}, purple curve) satellites and the differences between the two incident angles ($\theta_{\mathrm{TV12}} - \theta_{\mathrm{TV11}}$, color shading). TV signal intensity (unit: dBW) of (b) DirecTV-11 and (c) DirecTV-12. The sizes of grid boxes A and B are [39° N–40° N, 126° W–125° W] and [44° N–45° N, 126° W–125° W], respectively.

the change of the brightness temperature at 18.7 GHz ($\Delta T_{b,18p}^{\mathrm{TFI}}$) can be written separately for each of the two satellites

$$\Delta T_{b,18p}^{\mathrm{TFI}_{\mathrm{TV11}},\mathrm{phy}} = \Omega_{\mathrm{TV11},18p} \exp\left(-\frac{\alpha_{\mathrm{TV11}}^2}{2\sigma_{\mathrm{TV11}}^2}\right)$$
$$\Delta T_{b,18p}^{\mathrm{TFI}_{\mathrm{TV12}},\mathrm{phy}} = \Omega_{\mathrm{TV12},18p} \exp\left(-\frac{\alpha_{\mathrm{TV12}}^2}{2\sigma_{\mathrm{TV12}}^2}\right). \quad (2)$$

Taking a logarithmic operation of (2) gives the following relationships among the TFI correction terms, the glint angles, and the 3-dB beamwidth of the AMSR2 antenna:

$$\ln\left(\Delta T_{b,18p}^{\mathrm{TFI}_{\mathrm{TV11}},\mathrm{phy}}\right) = \ln(\Omega_{\mathrm{TV11},18p}) - \frac{1}{2\sigma_{\mathrm{TV11}}^2}\alpha_{\mathrm{TV11}}^2 \quad (3a)$$
$$\ln\left(\Delta T_{b,18p}^{\mathrm{TFI}_{\mathrm{TV12}},\mathrm{phy}}\right) = \ln(\Omega_{\mathrm{TV12},18p}) - \frac{1}{2\sigma_{\mathrm{TV12}}^2}\alpha_{\mathrm{TV12}}^2. \quad (3b)$$

In other words, $\ln(\Delta T_{b,18p}^{\mathrm{TFI,TV11}})$ is a linear function of the glint angle α_{TV11}^2, and the 3-dB beamwidth of the AMSR2 antenna σ_{TV11}^2 is simply the inverse slope of this linear fitting. The same is true for DirecTV-12. The values of α_{TV11}^2 and α_{TV12}^2 are finally obtained by minimizing the following cost functions:

$$J\left(\sigma_{\mathrm{TV11}}^2\right) = \sum_i \left(\ln\left(\Delta T_{b,18p}^{\mathrm{TFI}_{\mathrm{TV11}},\mathrm{phy}}\right) - \ln\left(\Delta T_{b,18p}^{\mathrm{TFI,reg}}\right)\right)_i^2 \tag{4a}$$

$$J\left(\sigma_{\mathrm{TV12}}^2\right) = \sum_i \left(\ln\left(\Delta T_{b,18p}^{\mathrm{TFI}_{\mathrm{TV12}},\mathrm{phy}}\right) - \ln\left(\Delta T_{b,18p}^{\mathrm{TFI,reg}}\right)\right)_i^2 \tag{4b}$$

where i represents data points, $\Delta T_{b,18p}^{\mathrm{TFI,reg}} = T_{b,18p}^{\mathrm{obs}} - T_{b,18p}^{\mathrm{reg}}$. $T_{b,18p}^{\mathrm{obs}}$ represents the AMSR2 actual observations at the 18.7-GHz channels. $T_{b,18p}^{\mathrm{reg}}$ is the TFI-free brightness temperature at 18.7 GHz predicted with sufficient accuracy using observations at other channels [15]. Outliers with $T_{b,18p}^{\mathrm{obs}} - T_{b,18p}^{\mathrm{reg}} < 3$ K are removed from the linear fitting.

Li *et al.* [15] argued that the portion of the natural radiation of a TFI channel, i.e., the TFI-free brightness temperature, can be predicted with sufficient accuracy using observations at other channels due to high channel correlations. Specifically, the TFI-free brightness temperature at the 18.7-GHz channels can be predicted according to

$$T_{b,18p}^{\mathrm{reg}} = a_0 + \sum_i a_i T_{b,i} + \sum_i b_i T_{b,i}^2 + c_1 \ln(290 - T_{b,23v}) + c_2 \ln(290 - T_{b,23h}) \tag{5}$$

where the subscript "p" can be either vertical or horizontal polarization. $T_{b,i}$ includes brightness temperature at channels at 6.925, 10.65, and 36.5 GHz of both polarizations. Channels at 18.7, 23.8, and 89.0 GHz are not involved in (5). a_i, b_i, and c_i are the regression coefficients to be determined. For each month, the observations over the entire globe were collected to train the coefficients, excluding those over land, coastlines, and sea ice and those where TFI glint angles are smaller than 30°. Over Europe, a similar regression model is developed to predict the TFI-free brightness temperatures at the 10.65-GHz channels, for which the left-hand side of (5) becomes $T_{b,10p}^{\mathrm{reg}}$ and $T_{b,18p}$ becomes the predictors in both the second and third terms at the right-hand side of (5). The regression coefficients are given in Table II. The regression errors are unbiased and have small standard deviations (e.g., $\leq$1.2 K) [15].

Fig. 3 provides two scatter plots of the natural logarithm of model differences (i.e., $\ln(T_{b,18h}^{\mathrm{obs}} - T_{b,18h}^{\mathrm{reg}})$) versus the squared AMSR2 glint angles α_{TV11}^2 [Fig. 3(a)] and α_{TV12}^2 [Fig. 3(b)]. It is shown that $\ln(T_{b,18h}^{\mathrm{obs}} - T_{b,18h}^{\mathrm{reg}})$ varies linearly with glint angles. The slopes of the regression lines in Fig. 5 are 1.242×10^{-2} and 0.527×10^{-2}, which give the following values of the 3-dB beamwidth of the AMSR2 antenna to the TV signals from DirecTV-11 and DirecTV-12: $\sigma_{\mathrm{TV11}} = 6.345°$ and $\sigma_{\mathrm{TV12}} = 9.734°$. A larger value of the 3-dB beamwidth implies more probable TFI occurrences.

TABLE II
REGRESSION COEFFICIENTS FOR MODEL PREDICTION OF BRIGHTNESS TEMPERATURE

Chan. [GHz]	Pol.	Coefficients							
10.65	H	a_0	a_1	a_2	a_3	a_4	a_5	a_6	c_1
		26.7619	0.82713	-0.46989	0.03655	0.00600	0.39156	-1.11107	10.7139
			b_1	b_2	b_3	b_4	b_5	b_6	c_2
			-0.00131	0.00135	0.00198	0.00024	-0.00124	0.00237	11.3386
	V	a_0	a_1	a_2	a_3	a_4	a_5	a_6	c_1
		-5.14359	0.05469	0.16220	-0.15875	0.89617	0.22439	-0.80272	15.3325
			b_1	b_2	b_3	b_4	b_5	b_6	c_2
			-0.00030	0.00111	0.00138	-0.00130	-0.00079	0.00178	-1.52765
18.7	H	a_0	a_1	a_2	a_3	a_4	a_5	a_6	c_1
		-181.979	-0.32332	0.16669	0.44787	2.22443	-0.05566	2.09958	-30.9304
			b_1	b_2	b_3	b_4	b_5	b_6	c_2
			0.00046	-0.00043	0.00086	-0.00578	0.00124	-0.00545	-4.88228
	V	a_0	a_1	a_2	a_3	a_4	a_5	a_6	c_1
		-103.249	-0.26636	0.15016	0.17965	0.68760	-0.36495	2.55719	-4.03127
			b_1	b_2	b_3	b_4	b_5	b_6	c_2
			0.00034	-0.00005	0.00008	-0.00100	0.00114	-0.00530	-16.0483

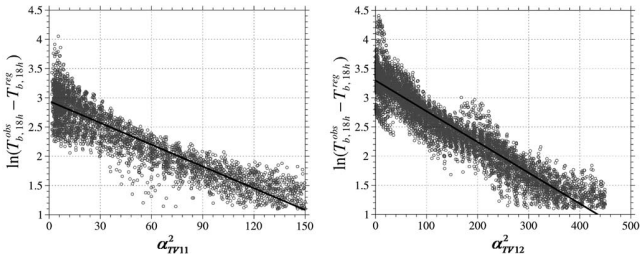

Fig. 3. Scatter plots of $\ln(T_{b,18h}^{\mathrm{obs}} - T_{b,18h}^{\mathrm{reg}})$ versus squared glint angle (α^2) with respect to DirecTV-11 (α_{TV11}^2, left panel) and DirecTV-12 (α_{TV11}^2, right panel) for TFI-affected data in 2014 within two 1° × 1° boxes [see boxes A and B in Fig. 2(a)] in clear-sky conditions. The linear regression line is also indicated.

Once the unknown parameters α_{TV11} and α_{TV12} are determined, the background TFI intensity due to the TV signals of DirecTV-11 and DirecTV-12, $\Omega_{\mathrm{TV11},18p}$ and $\Omega_{\mathrm{TV12},18p}$, can then be determined using AMSR2 data in 2014. It is pointed out that both background TFI intensities (i.e., $\Omega_{\mathrm{TV11},18p}$ and $\Omega_{\mathrm{TV12},18p}$) have a linear relationship to $\Delta T_{b,18p}^{\mathrm{TFI}_{\mathrm{TV11}},\mathrm{phy}}$. To obtain a spatial distribution of any of $\Omega_{\mathrm{TV11},18p}$ and $\Omega_{\mathrm{TV12},18p}$, the area over the U.S. and its coastal areas (15° N–70° N, 140° W–50° W) is divided into $0.25° \times 0.25°$ grid boxes. The field of $\Omega_{\mathrm{TV11},18p}$ and $\Omega_{\mathrm{TV12},18p}$ within each grid box can be generated by minimizing the following cost function:

$$J(\Omega_{\mathrm{TV11},18p}, \Omega_{\mathrm{TV12},18p}) = \sum_i \left(\Delta T_{b,18p}^{\mathrm{TFI,phy}} - \Delta T_{b,18p}^{\mathrm{TFI,reg}}\right)_i^2 \tag{6}$$

with all TFI-affected AMSR2 observations in 2014 in the grid box, where TFI data are defined by $T_{b,18p}^{\mathrm{obs}} - T_{b,18p}^{\mathrm{reg}} > 3$ K. The spatial distributions of the data count of the TFI pixels within each $0.25° \times 0.25°$ grid box for all of the data in 2014 and the TFI intensity field for the 18.7-GHz channel at horizontal polarization from DirecTV-12 ($\Omega_{\mathrm{TV12},18h}$), which is obtained by minimizing (6), are presented in Fig. 4(a) and (b),

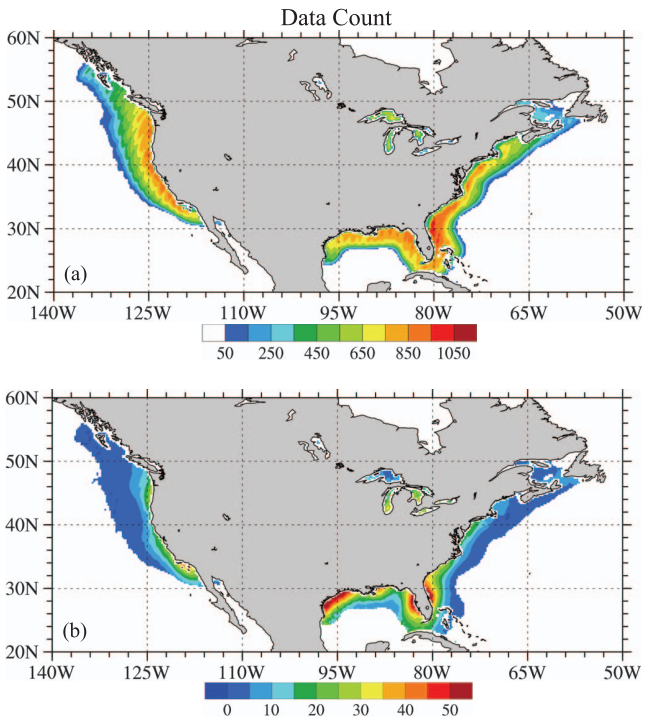

Fig. 4. Spatial distributions of (a) the data count of the TFI-affected AMSR2 pixels and (b) the TFI intensity for the 18.7-GHz channel at horizontal polarization from DirecTV-12 ($\Omega_{\mathrm{TV12},18h}$, unit: K) derived from the empirical model for TFI correction.

respectively. Fig. 4(b) can be compared with Fig. 2(c) to find out that the characteristic spatial variations of the TFI intensity of $\Omega_{\mathrm{TV12},18h}$, being the strongest in the coastal areas of Miami and weaker in the West Coast of the U.S. [Fig. 4(b)], are consistent with those of the TV signal intensity of DirecTV-12 [Fig. 2(c)].

B. Empirical Model for TFI Correction Over Europe

Around Europe, the AMSR2 dual-polarized X-band channels at 10.65 GHz could have TFI from Hispasat 1E, Eutelsat West 7A, and Thor 6, and Hot Bird 13B, Astra 2E, and Thor 6 satellites (Table III and Fig. 1). The spatial distributions of the incident angles of these five European TV satellites are provided in Fig. 5. At a fixed location, the AMSR2 X-band channels could be interfered with the ocean-reflected TV signals from multiple TV satellites varying from one to five and of different strengths. Different TV satellites have different focusing areas. Fig. 6 shows the TV signal intensity of Hispasat 1E, Eutelsat West 7A, Thor 6, Hot Bird 13B, and Astra 2E. It is shown that Astra 2E transmits signals mainly to a limited area surrounding the U.K., Hot Bird 13B covers a much broader area of Greater Europe, and Thor 6 focuses to high latitudes.

The TFI correction model over Europe is similar to that described in Section III-A. When selecting TFI data samples for determining the 3-dB beamwidth parameter (σ) of the five European TV satellites, each TV satellite's focusing area needs to be taken into consideration. For example, the TFI given rise by Astra 2E will occur in a limited area surrounding the U.K. Therefore, considering the distributions of both the incident

TABLE III
INTERFERING GEOSTATIONARY TV SATELLITES

Longitude	TV Satellites	Focusing Areas	Interfered Channel (GHz)
102.8W	DirecTV-10	North America	18.7
	DirecTV-12	North America	18.7
99.2W	DirecTV-11	North America	18.7
30.0W	Hispasat 1E	South Europe	10.65
7.2W	Eutelsat 7 West A	North Africa	10.65
0.8W	Thor 6	North Europe	10.65
13.0E	Hot Bird 13B	Greater Europe	10.65
	Hot Bird 13C	Greater Europe	10.65
28.2E	Astra 2E	United Kingdom	10.65

Detailed information available at: http://www.lyngsat.com.

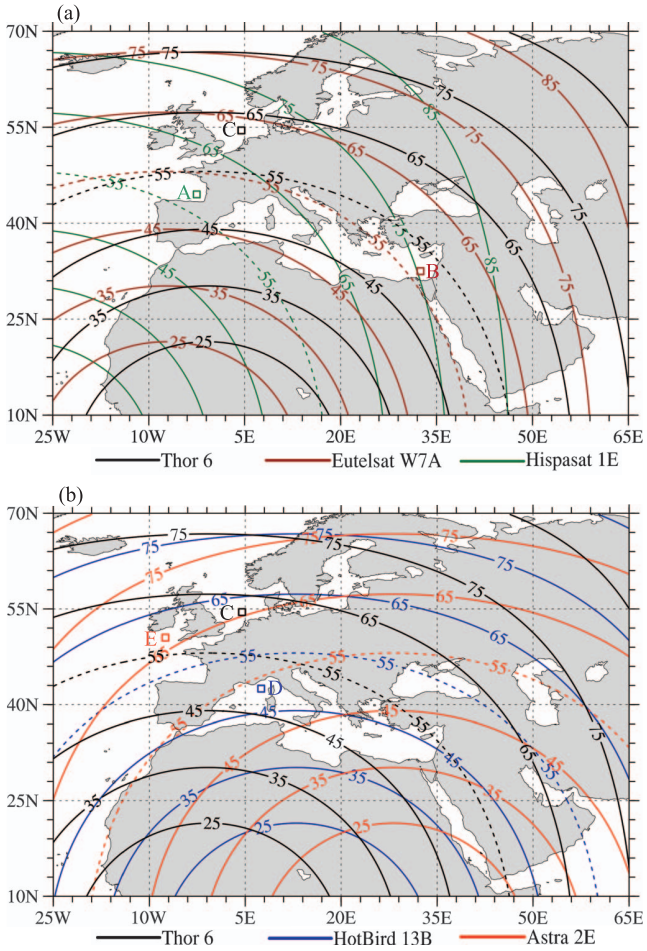

Fig. 5. Spatial distributions of the incident angles (unit: degrees) of (a) Hispasat 1E, Eutelsat West 7A, and Thor 6 and (b) Hot Bird 13B, Astra 2E, and Thor 6. The sizes of grid boxes A–E are [44° N–45° N, 3° W–2° W] for Hispasat 1E, [32° N–33° N, 33° E–33° E] for Eutelsat West 7A, [54° N–55° N, 4° E–5° E] for Thor 6, [42° N–43° N, 7° E–8° E] for Hot Bird 13B, and [50° N–51° N, 8° W–7° W] for Astra 2E.

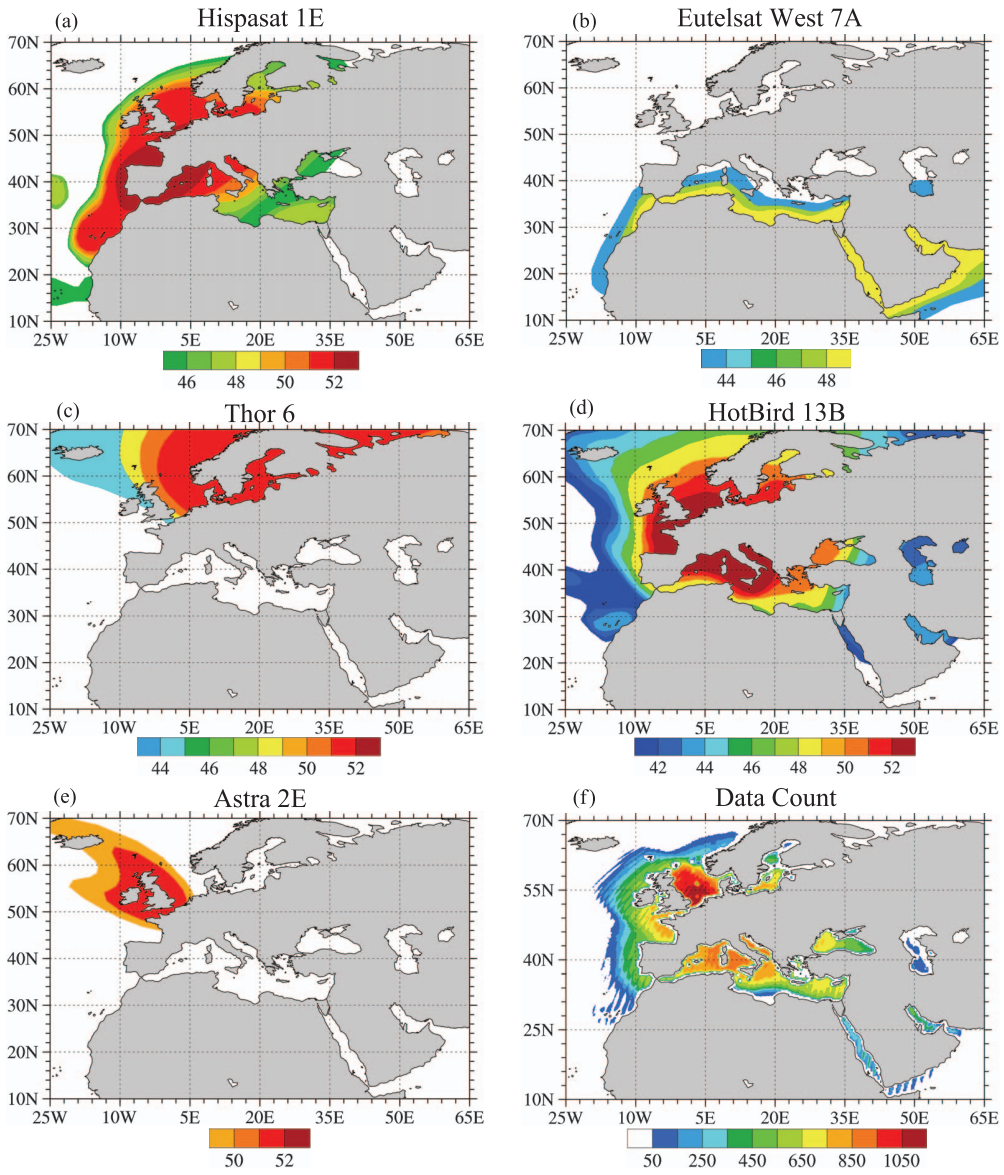

Fig. 6. (a)–(e) TV signal intensities (unit: dBW) of Hispasat 1E, Eutelsat West 7A, Thor 6, Hot Bird 13B, and Astra 2E. Spatial distributions of the data count of the TFI-contaminated observations at a 10.65-GHz channel within a $0.25^\circ \times 0.25^\circ$ grid box in 2014.

angles (Fig. 5) and the TV signal intensities [Fig. 6(a)–(e)], the geographical locations selected for determining the antenna pattern parameter of the five satellites (σ_i, $i = 1, 2, \ldots, 5$) are shown in Fig. 5. All TFI-affected AMSR2 observations in 2014 that fall into each of the five boxes are extracted to calculate the 3-dB beamwidth parameters. The values of the 3-dB beamwidth of the AMSR2 antenna to the TV signals are the following: 5.631 for Hispasat 1E, 6.172 for Eutelsat West 7A, 6.898 for Thor 6, 9.068 for Hot Bird 13B, and 5.308 for Astra 2E.

Once the AMSR2 antenna's 3-dB beamwidths to the reflected TV signals of the five European satellites are obtained, the background TFI intensities ($\Omega_{i,10p}$, $i = 1, 2, \ldots, 5$) can be obtained by minimizing the following cost function:

$$J(\Omega_{1,10p}, \Omega_{2,10p}, \ldots, \Omega_{5,10p}) = \sum_i \left(\Delta T_{b,10p}^{\mathrm{TFI,phy}} - \Delta T_{b,10p}^{\mathrm{TFI,reg}}\right)_i^2 \quad (7)$$

where i represents the TFI data points within each $0.25^\circ \times 0.25^\circ$ grid box. The total number of TFI-affected data in each $0.25^\circ \times 0.25^\circ$ grid box during 2014 is shown in Fig. 6(f). It is shown that TFI occurs most frequently over the North Sea area between U.K. and Norway due to the fact that this is an area that is covered with strong TV signals from three different TV satellites: Thor 6, Hot Bird 13B, and Astra 2E.

IV. Applications of the Two Empirical Models for AMSR2 TFI Correction

A. Impacts on AMSR2 18.7 GHz Over the U.S.

The amount of natural radiation in AMSR2 observed brightness temperatures at K-band channels over interfered pixels is concealed by the reflected TV signals. An example is given in Fig. 7, which shows the AMSR2 observed brightness temperature [$T_{b,18h}^{\mathrm{obs}}$; Fig. 7(a)], the regression-model-predicted

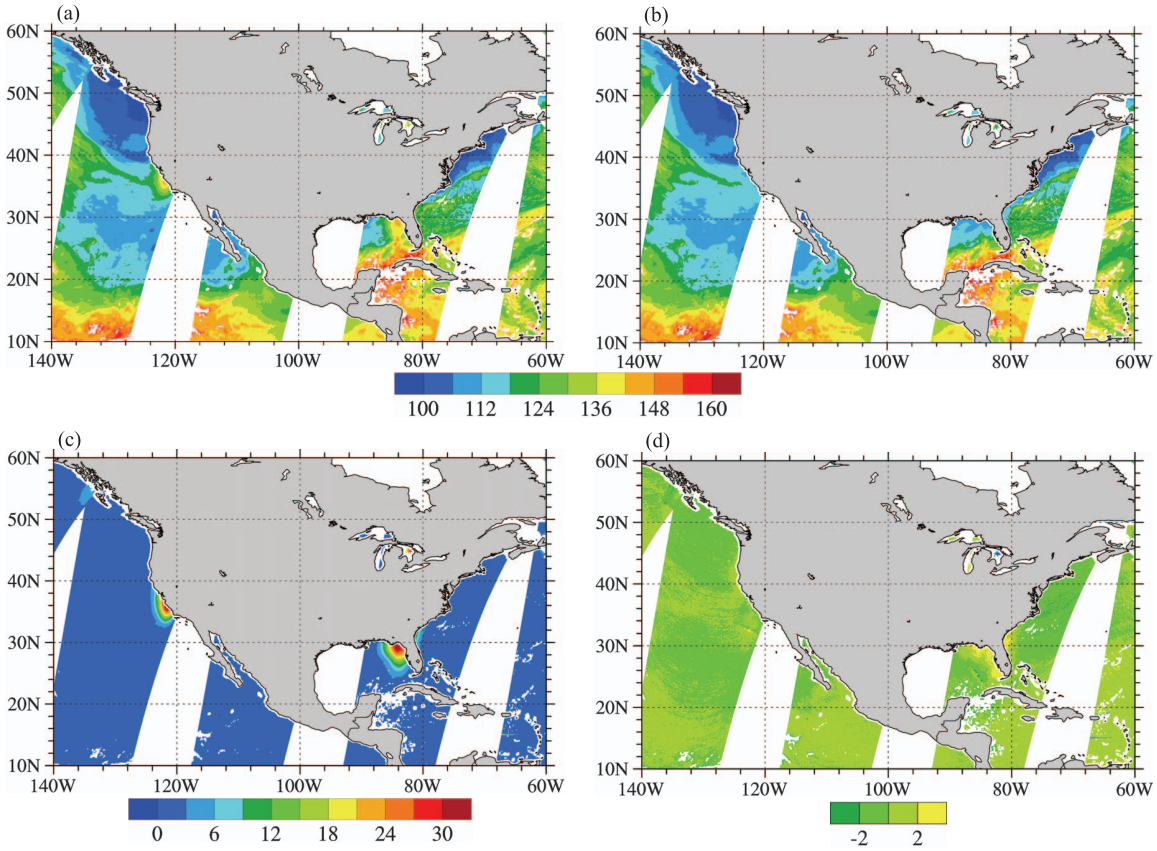

Fig. 7. (a) AMSR2 observed and (b) regression-model-predicted brightness temperatures (unit: K) of the 18.7-GHz channel at horizontal polarization. (c) TFI correction (unit: K). (d) Differences of brightness temperatures between AMSR2 observations with TFI correction term incorporated and the regression model simulation of 18.7 GHz at horizontal polarization on January 4, 2014.

brightness temperatures [$T_{b,18h}^{\mathrm{reg}}$; Fig. 7(b)] of the 18.7-GHz channel at horizontal polarization, the TFI correction calculated by the empirical model (1) [$\Delta T_{b,18h}^{\mathrm{TFI,phy}}$; Fig. 7(c)], and the differences of the brightness temperatures between AMSR2 observations with TFI correction term incorporated and the regression model simulation [$(T_{b,18h}^{\mathrm{obs}} - \Delta T_{b,18h}^{\mathrm{TFI,phy}}) - T_{b,18h}^{\mathrm{reg}}$; Fig. 7(d)] of the descending node on January 4, 2014. Over an area located at the West Coast of the U.S. in the east half of the AMSR2 swath and another area located at the west cost of Miami in the west half of the AMSR2 swath, the TFI raises the observed brightness temperatures by more than 30 K. After TFI correction, the differences between AMSR2 observations and regression model simulations are no more than ± 4 K. How much impacts does the TFI correction have on geophysical retrieval products involving 18.7-GHz channels?

LWP and TPW can be retrieved with multiple microwave window channels, so that the absorptions of the atmosphere and the emission of the surface can be removed. The LWP and TPW can be retrieved either with brightness temperature observations at the 18.7- and 23.8-GHz channels or with those at the 36.5- and 23.8-GHz channels, shown by the following equations:

$$\mathrm{LWP}_{18} = A_{01}\mu\left[\ln(T_s - T_{b,18}) - A_{11}\ln(T_s - T_{b,23}) - A_{21}\right] \tag{8a}$$

$$\mathrm{LWP}_{36} = A_{02}\mu\left[\ln(T_s - T_{b,36}) - A_{12}\ln(T_s - T_{b,23}) - A_{22}\right] \tag{8b}$$

$$\mathrm{TPW}_{18} = B_{01}\mu\left[\ln(T_s - T_{b,18}) - B_{11}\ln(T_s - T_{b,23}) - B_{21}\right] \tag{8c}$$

$$\mathrm{TPW}_{36} = B_{02}\mu\left[\ln(T_s - T_{b,36}) - B_{12}\ln(T_s - T_{b,23}) - B_{22}\right] \tag{8d}$$

where A_{ij} and B_{ij} ($i = 0, 1, 2$, $i = 1, 2$) are coefficients and μ is . . ..

At any locations, the same geophysical variable retrieved with observations at either frequency channels is expected to have similar variations. However, the 18.7-GHz channels are subject to TFI, and the 36.5-GHz channels are free of TFI. As a consequence, the retrieval products of both LWP and TPW from the 18.7-GHz channels could have errors in the presence of TFI signals. The impact of TFI correction derived from the empirical model can be evaluated by comparing the same variable retrieved with K-band brightness temperatures before and after the correction with that retrieved from the 36.6-GHz channels. Fig. 8 shows the spatial distributions of the TPW retrieved from AMSR2 brightness temperature observations at 36.5 GHz [$\mathrm{TPW}_{36.5}$; Fig. 8(a)], the TPW retrieved from AMSR2 brightness temperature observations using 18.7-GHz ($\mathrm{TPW}_{18.7}$) channels without [Fig. 8(b)] and with [Fig. 8(c)] TFI correction, and the TPW differences ($\mathrm{TPW}_{36.5} - \mathrm{TPW}_{18.7}$) between 36.5-GHz retrieval and 18.7-GHz retrieval without [Fig. 8(d)] and with [Fig. 8(e)] TFI correction incorporated using the descending data on January 4, 2014. It is shown

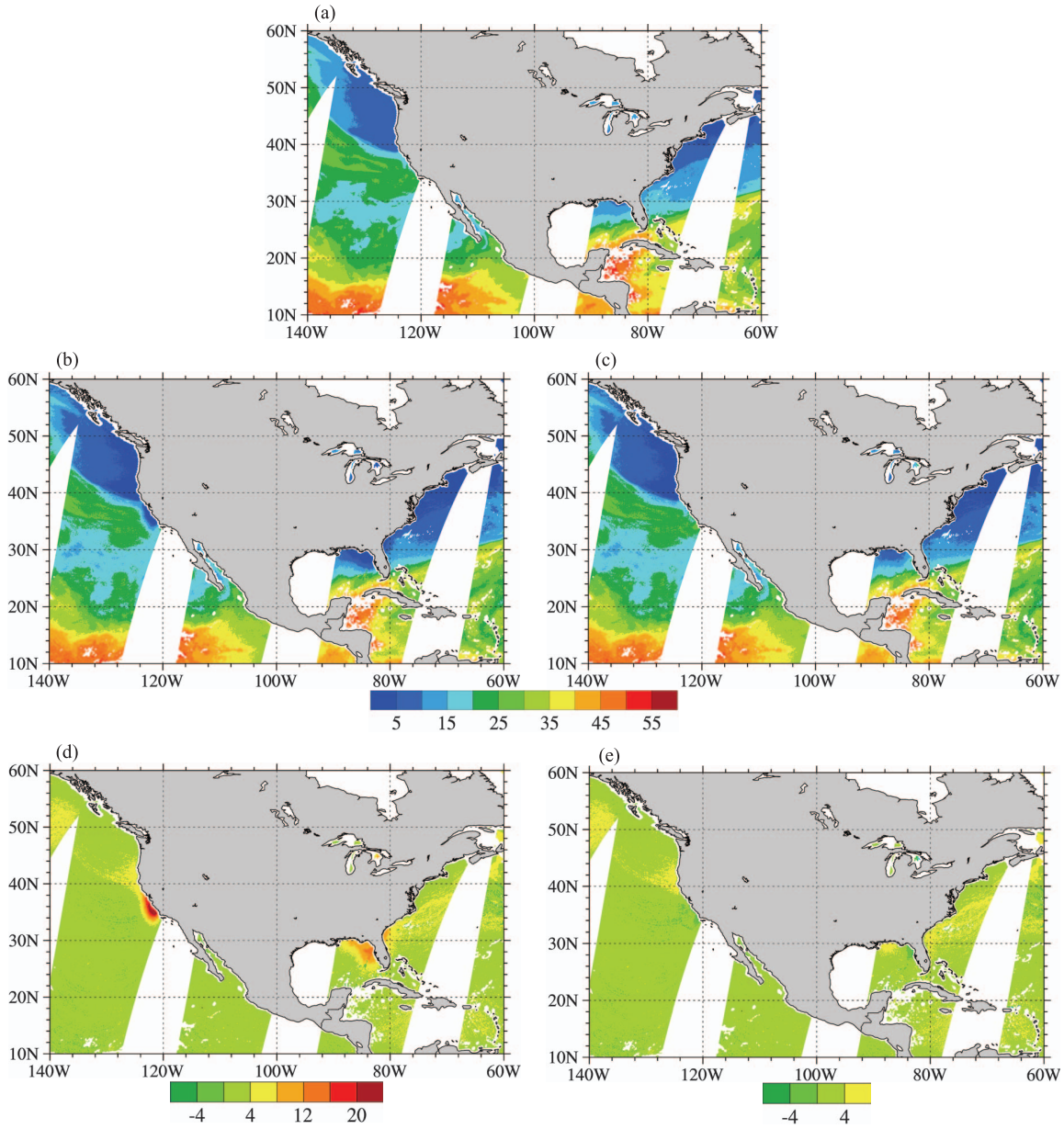

Fig. 8. Spatial distributions of (a) TPW (unit: kg m^{-2}) retrieved from AMSR2 brightness temperature observations of 36.5 GHz ($TPW_{36.5}$), (b) and (c) TPW retrieved from AMSR2 brightness temperature observations of 18.7 GHz ($TPW_{18.7}$) channels, and (d) and (e) TPW differences between retrievals from the two different frequencies ($TPW_{36.5} - TPW_{18.7}$) without (left panels) and with (right panels) TFI correction on January 4, 2014.

that, over the coastal areas with TFI [Fig. 7(c)], the TPW retrieved from 18.7 GHz is more than 20 kg m^{-2}, smaller than that with TFI correction or retrieved from TFI-free channels at 36.5 GHz [Fig. 8(d)]. The differences of TPWs between 36.5-GHz retrieval and 18.7-GHz retrieval with TFI correction or over areas without TFI are usually less than ± 4 kg m^{-2}. The impacts of TFI on LWP retrieval are also significant (Fig. 9). The TFI signals cause a false amount of LWP for more than 0.5 kg m^{-2}. The differences of LWPs between 36.5-GHz retrieval and 18.7-GHz retrieval are usually less than ± 4 kg m^{-2} over areas without TFI. The differences of LWPs between 36.5-GHz retrieval and 18.7-GHz retrieval with TFI correction or over TFI-free areas are larger over areas with larger LWP.

Monthly variations of biases are calculated from the differences between AMSR2 observed and regression-model-predicted brightness temperatures of the 18.7-GHz channel at horizontal and vertical polarizations for all clear-sky data in 2014 with the AMSR2 glint angle being less than or equal to 30° before and after TFI correction calculated by the empirical models developed in this study. The percentage number of the TFI-affected AMSR2 pixels in each month of 2014 is also given in Fig. 10. It is shown that there is about 3% of TFI-affected data with glint angle $\alpha \leq 30°$. The monthly mean differences between AMSR2 observations without TFI correction and regression-model-predicted brightness temperature of the 18.7-GHz channel at horizontal polarization vary from 5.5

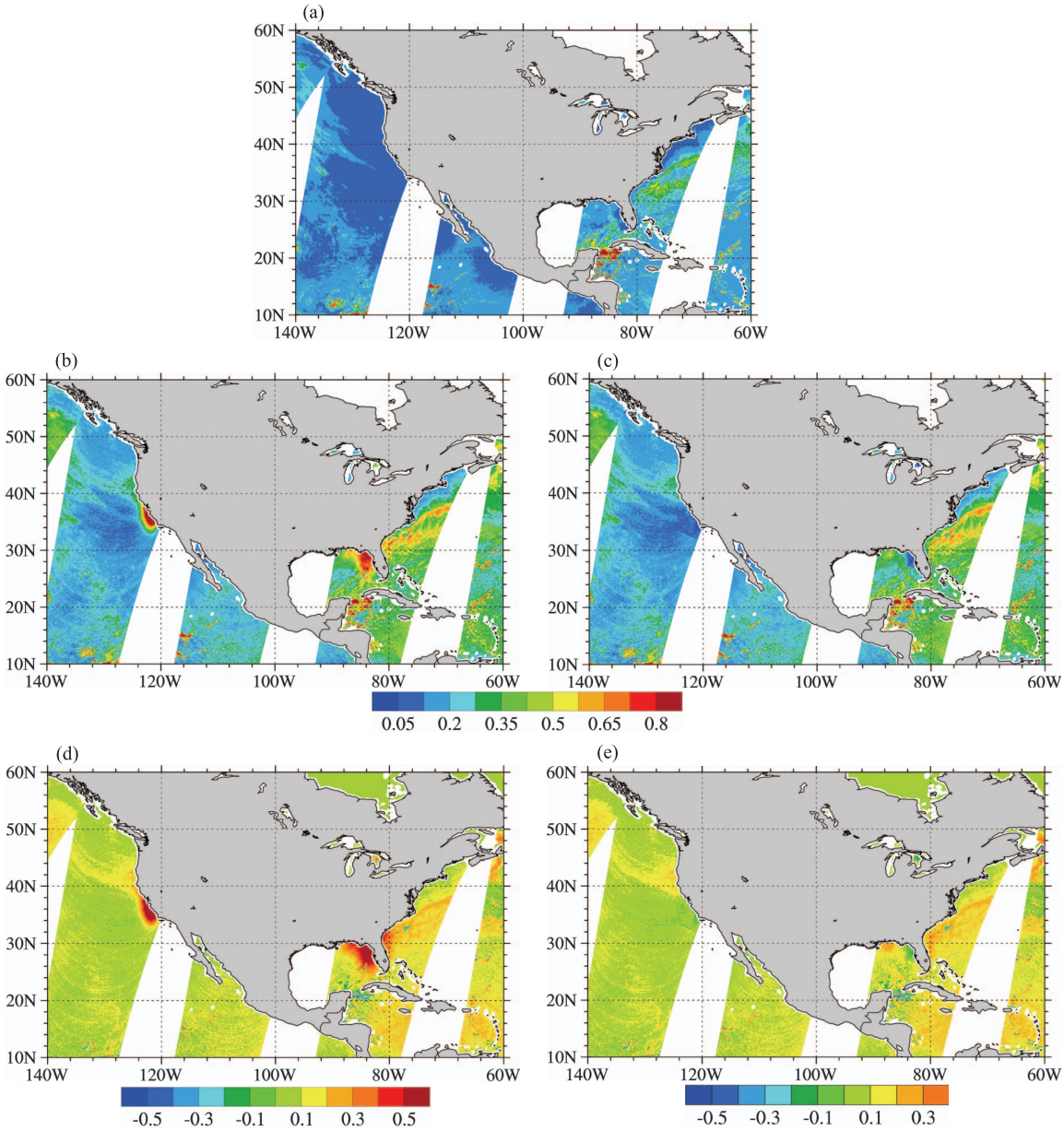

Fig. 9. Same as Fig. 8 except for LWP (unit: kg m^{-2}).

to 6.5 K in 2014. After TFI correction, the monthly mean differences of the 18.7-GHz channel at horizontal polarization are significantly reduced in magnitude, with its values varying between −0.25 K and −0.7 K. The TFI-introduced biases for the 18.7-GHz channel at vertical polarization are around 1.5 K, which is smaller than at the horizontal polarization. After TFI correction, the monthly biases of the 18.7-GHz channel at vertical polarization are reduced to between −0.1 K and −0.3 K.

As illustrated in Fig. 1, TFI arising from geostationary satellite TV signals' being picked up by AMSR2 will travel through the entire atmosphere twice. Thus, TFI is subject to atmospheric attenuations. Since the reflection of the TV signals occurs at the ocean surface, the amount of reflected microwave signals will be influenced by the surface roughness. Under windy circumstances, the ocean surface can become rougher than the calm ocean surface. Fig. 11 shows the differences between the TFI intensities yielded by the regression method and the modeled TFI intensities with respect to the SSWs and TPW. It seems that the TFI model will slightly overestimate the interference intensity when either SSW or TPW is high if the surface roughness and/or atmospheric attenuations are not considered as the case for the current model. The neglect of surface roughness and atmospheric attenuation might be the reason for the slight negative biases in the monthly mean of differences between TFI intensities from the regression method and those from the model shown in Fig. 10.

B. *Impacts on AMSR2 10.65 GHz Over Europe*

Over Europe, the impacts of TFI correction using the established empirical model on AMSR2 10.65-GHz channels are also significant and positive. As mentioned previously, there are

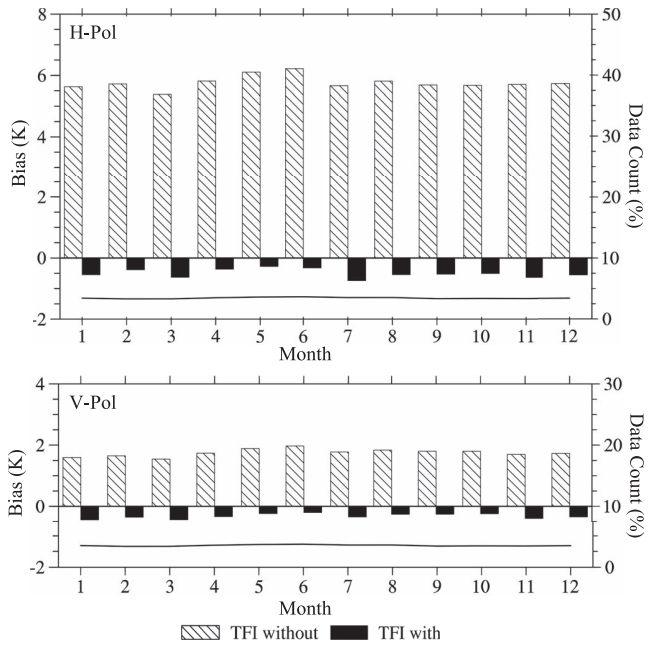

Fig. 10. Monthly variations of biases (unit: K) calculated from the differences between AMSR2 observed and regression-model-predicted brightness temperatures (unit: K) of the 18.7-GHz channel at horizontal (top panel) and vertical (bottom panel) polarizations for global clear-sky data in 2014 with the AMSR2 glint angle being less than or equal to 30° before (dashed bar) and after (solid bar) TFI correction. The percentage number (unit: %) of TFI-affected AMSR2 pixels in each month of 2014 is indicated by the black curve.

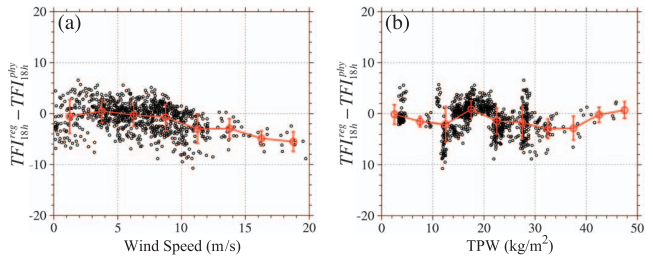

Fig. 11. Scatter plot of $T^{\mathrm{obs}}_{b,18h} - T^{\mathrm{reg}}_{b,18h}$ with respect to the surface wind speed and TPW. Data are selected within the geographical range of [39° N–41° N, 127° W–125° W] in January and February 2014. The glint angles with respect to DirecTV-12 are between 8° and 10°. The red circles and red lines are the mean and error bar at the 2.5 (left panel) and 5 (right panel) intervals.

five TV satellites that could introduce TFI to these two X-band channels depending on the locations of the AMSR2 pixels, the TV signal intensities of the five TV satellites [Fig. 6(a)–(e)], and the AMSR2 glint angles with respect to the five TV satellites. An example is provided to show the AMSR2 glint angles with respect to the five TV satellites over Europe (i.e., Hispasat 1E, Eutelsat West 7A, Thor 6, Hot Bird 13B, and Astra 2E) for the descending node on March 2, 2014 [Fig. 12(a)–(e)]. Due to the different geographical locations of the five TV satellites (see Table III), the AMSR2 glint angles with respect to the five TV satellites over Europe are significantly different. With the same AMSR2 observation geometry and the given TV signal intensities of the five TV satellites [Fig. 6(a)–(e)], the TFI correction calculated from the empirical model [Fig. 12(f)] seems to capture the TFI reasonably well. This is further confirmed by a comparison of results of TFI correction calculated from

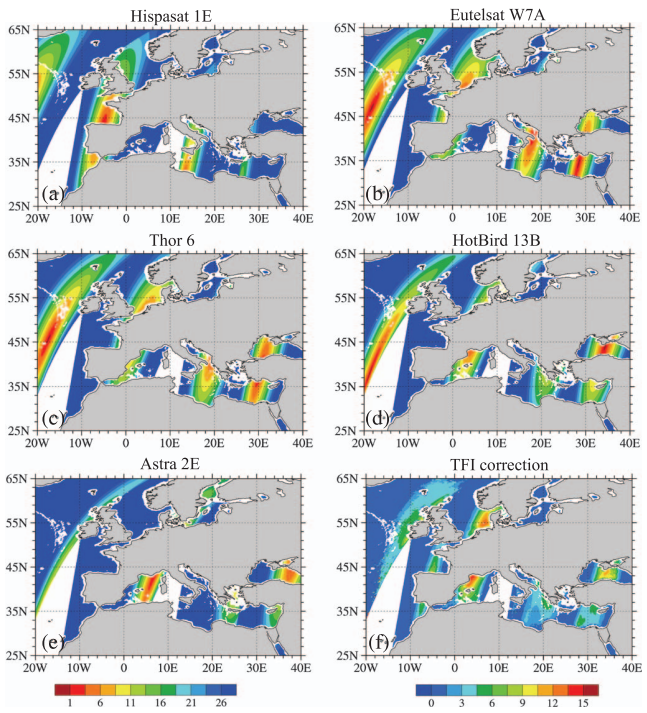

Fig. 12. (a)–(e) AMSR2 glint angles (unit: degrees) with respect to the five TV satellites over Europe (i.e., Hispasat 1E, Eutelsat West 7A, Thor 6, Hot Bird 13B, and Astra 2E) and (f) TFI correction (unit: K) as a combined TFI impacts from all five European satellites for the descending node on March 2, 2014.

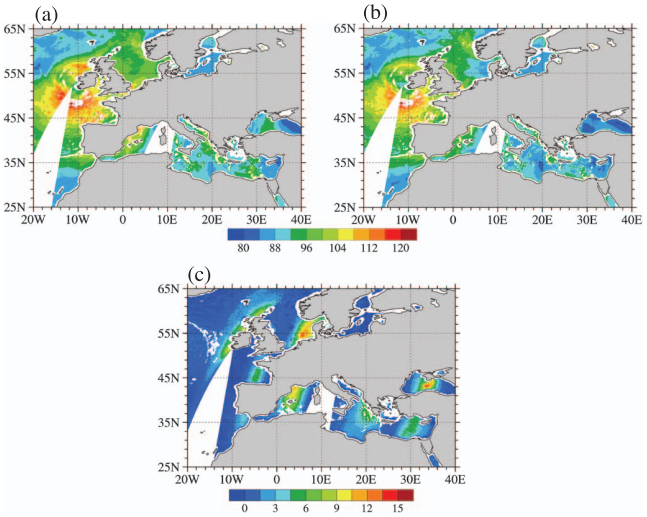

Fig. 13. (a) AMSR2 observed and (b) regression-model-predicted brightness temperatures (unit: K) of the 10.65-GHz channel at horizontal polarization on March 2, 2014. (c) Differences between (b) and (a).

the empirical model in Fig. 12(f) with the differences between AMSR2 observations [Fig. 13(a)] and the model-predicted brightness temperatures using a regression equation for the 10.65-GHz channel at horizontal polarization [i.e., similar to (5); Fig. 13(c)] on March 2, 2014.

A statistical evaluation of an overall performance of the empirical models for TFI correction at X-bands is provided in Fig. 14. There are about 10% of TFI-affected data with glint angle $\alpha \leq 30°$. Similar to the results in Fig. 10 for the K-band

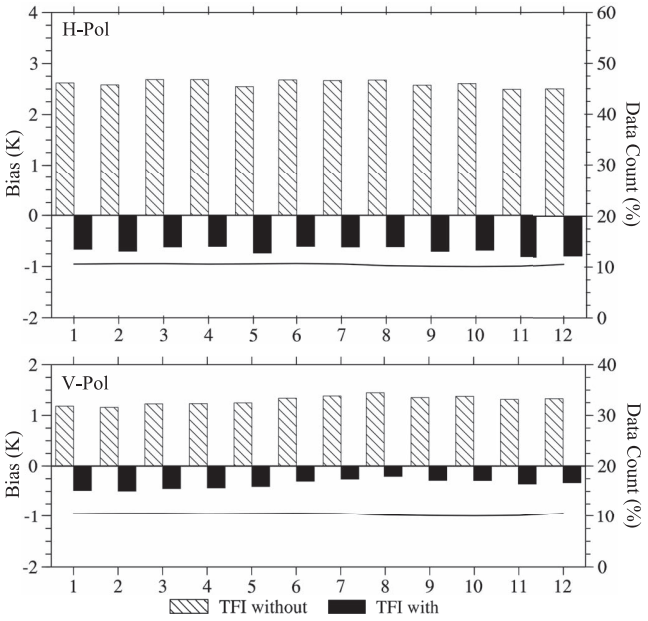

Fig. 14. Same as Fig. 10 except at the 10.65-GHz channels.

channels over the U.S., the presence of TFI introduces positive biases to the X-band channels over Europe, and the remaining biases are negative after TFI correction. The monthly biases are around 2.5 K and 1.2 K for the 10.65-GHz channels at horizontal and vertical polarizations, respectively. After TFI correction, these biases are reduced to about −0.5 K and −0.3 K.

V. Summary and Conclusion

In the presence of TFI, the amount of natural radiation emitted by the Earth surface is concealed by the energy from the reflected TV signals. The TFI detection prevents erroneous geophysical retrieval products from being produced by discarding the TFI-affected AMSR2 data. This study aims not only to detect the occurrence of TFI but also to correct the TFI so that these TFI-affected data can be made useful for geophysical variable retrieval. The occurrence of TFI from a particular TV satellite depends on the glint angle and the background TV signal intensity at the AMSR2 observation location. The contribution of the reflected TV signals to an AMSR2 observation at a specific channel can be calculated by an empirical model developed in this research given the AMSR2 glint angle with respect to those TV satellites that can have an effect to the AMSR2 pixel location. The glint angles can be accurately assessed with the instrument's observation geometry. This empirical model can predict the features of oceanic TFI that enable the AMSR2 observations from the natural radiation recovered even at the TV interfered locations. It is shown that positive biases in AMSR2 data are significantly reduced after TFI correction. The TFI-induced errors in the geophysical retrieval products can be considerably reduced over the TFI-contaminated regions so that variations of the retrieval variables are consistent with the vicinity regions. The background TV signal intensity field, once determined, is fixed for future applications as long as the same geostationary TV satellites are functioning. It is worth emphasizing that the TFI-correction model proposed in this study does not rely on any radiance observations, which was not the case in all previous studies.

It is pointed out that the effects of surface roughness induced by SSW as well as atmospheric attenuations by water vapor on reflected TV signals are not considered in the empirical model that was developed and tested in this study. Neglect of these two factors results in small negative biases of this TFI correction model. Further investigations on accounting quantitatively for the effects of surface roughness and atmospheric attenuation will be carried out in a follow-on study.

Acknowledgment

The authors would like to thank Dr. H. Yang for the several inspiring discussions at the early stage of this paper.

References

[1] M. Kachi *et al.*, "Status of GCOM-W1/AMSR2 development and science activities sensors, systems, and next-generation satellites XII," in *Proc. SPIE*, 2008, vol. 7106, pp. 1–8.

[2] T. Wilheit, C. D. Kummerow, and R. Ferraro, "NASDA rainfall algorithms for AMSR-E," *IEEE Trans. Geosci. Remote Sens.*, vol. 41, no. 2, pp. 204–214, Feb. 2003.

[3] E. G. Njoku and L. Li, "Retrieval of land surface parameters using passive microwave measurements at 6–18 GHz," *IEEE Trans. Geosci. Remote Sens.*, vol. 37, no. 1, pp. 79–93, Jan. 1999.

[4] E. G. Njoku, T. J. Jackson, V. Lakshmi, T. K. Chan, and S. V. Nghiem, "Soil moisture retrieval from AMSR-E," *IEEE Trans. Geosci. Remote Sens.*, vol. 41, no. 2, pp. 215–229, Feb. 2003.

[5] R. E. Kelly, A. T. Chang, L. Tsang, and J. L. Foster, "A prototype AMSR-E global snow area and snow depth algorithm," *IEEE Trans. Geosci. Remote Sens.*, vol. 41, no. 2, pp. 230–242, Feb. 2003.

[6] X. Zou, J. Zhao, F. Weng, and Z. Qin, "Detection of radio-frequency interference signal over land from FY-3B Microwave Radiation Imager (MWRI)," *IEEE Trans. Geosci. Remote Sens.*, vol. 50, no. 12, pp. 4994–5003, Dec. 2012.

[7] J. Zhao, X. Zou, and F. Weng, "WindSat radio-frequency interference signature and its identification over Greenland and Antarctic," *IEEE Trans. Geosci. Remote Sens.*, vol. 51, no. 9, pp. 4830–4839, Sep. 2013.

[8] X. Zou, X. Tian, and F. Weng, "Detection of television frequency interference with satellite microwave imager observations over oceans," *J. Atmos. Ocean. Technol.*, vol. 31, no. 12, pp. 2759–2776, Dec. 2014.

[9] I. S. Adams, M. H. Bettenhausen, P. W. Gaiser, and W. Johnston, "Identification of ocean-reflected radio frequency interference using WindSat retrieval chi-square probability," *IEEE Geosci. Remote Sens. Lett.*, vol. 7, no. 2, pp. 406–410, Apr. 2010.

[10] D. Truesdale, "A probability distribution method for detecting radio-frequency interference in WindSat observations," *IEEE Trans. Geosci. Remote Sens.*, vol. 51, no. 6, pp. 3780–3788, Jun. 2013.

[11] W. M. Wiltshire, M. D. Nilsson, and F. B. Campbell, "Application for Authorization to Launch and Operate DirecTV 10, a Partial Replacement Ka-Band Satellite, at 103 deg.," Federal Communications Commission, WL, FCC form 312, Exhibit 43, Tech. Rep.

[12] F. J. Wentz and T. Meissner, *Algorithm Theoretical Basis Document (ATBD) AMSR Ocean Algorithm*, 2nd Ed. Santa Rosa, CA, USA: IEEE, 2000.

[13] F. Weng and N. C. Grody, "Retrieval of cloud liquid water using the Special Sensor Microwave Imager (SSM/I)," *J. Geophys. Res.*, vol. 99, no. D12, pp. 25 535–25 551, 1994.

[14] B. Yan and F. Weng, "Application of AMSR-E measurements for tropical cyclone predictions. Part I: Retrieval of sea surface temperature and wind speed," *Adv. Atmos. Sci.*, vol. 25, pp. 227–245, 2008.

[15] L. Li, P. W. Gaiser, M. Bettenhausen, and W. Johnston, "WindSat radio-frequency interference signature and its identification over land and ocean," *IEEE Trans. Geosci. Remote Sens.*, vol. 44, no. 3, pp. 530–539, Mar. 2006.

[16] H. Yang and F. Weng, "Corrections for on-orbit ATMS lunar contamination," *IEEE Trans. Geosci. Remote Sens.*, vol. 54, no. 4, pp. 1918–1924, Apr. 2016.

[17] T. Kawanishi *et al.*, "The Advanced Microwave Scanning Radiometer for the Earth Observing System (AMSR-E), NASA's contribution to the EOS for global energy and water cycle studies," *IEEE Trans. Geosci. Remote Sens.*, vol. 41, no. 2, pp. 184–194, Feb. 2003.
[18] R. Poisel, *Antenna Systems and Electronic Warfare Applications*. Norwood, MA, USA: IEEE, 2012, pp. 363–416.
[19] D. McKague, J. J. Puckett, and C. Ruf, "Characterization of K-band radio frequency interference from AMSR-E, WindSat and SSM/I," in *Proc. IEEE IGARSS*, 2010, pp. 2492–2494.
[20] S. Martin, *An Introduction to Ocean Remote Sensing*. New York, NY, USA: IEEE, 2004.

Xiaoxu Tian received the B.S. and M.S. degrees from Florida State University, Tallahassee, FL, USA, in 2012 and 2014, respectively.

He is currently a Graduate Research Assistant with the Department of Atmospheric and Oceanic Science and Earth System Science Interdisciplinary Center, University of Maryland, College Park, MD, USA. The area of his research includes detection and mitigation of radio frequency interference in microwave radiometers and atmospheric temperature retrievals with observations of microwave temperature sounders.

Xiaolei Zou received the Ph.D. degree in meteorology from the Institute of Atmospheric Physics, Academia Sinica, Beijing, China, in 1988.

From 1989 to 1993, she developed the 4D-Var system of the National Meteorological Center medium-range global model (now the National Center for Environmental Prediction) medium-range forecast model with full physics. From 1993 to 1997, she developed the MM5 4D-Var system and worked on GPS radio occultation data assimilation at the National Center for Atmospheric Research. She was a Professor with the Department of Earth, Ocean, and Atmospheric Science, Florida State University, Tallahassee, FL, USA, from 1997 to 2014. Since the fall of 2014, she has been with the Earth System Science Interdisciplinary Center, University of Maryland, College Park, MD, USA. She has published over 121 papers in peer-reviewed journals. Her research focuses on satellite data assimilation for improving quantitative precipitation forecasts and hurricane track and intensity forecasts, as well as satellite calibration and climate trend studies.

Dr. Zou was the recipient of the 2008 American Meteorological Society Fellow Award for her outstanding contributions to the applications of satellite data in the numerical weather prediction models and the education in data assimilation.